07,05

Synthesis, characterizations and magnetic properties of new $(MnS)_{1-x}(TiN)_x$ compounds

© G.M. Abramova[1], M.M. Syrokvashin[2,3], S.A. Skorobogatov[1], D.A. Velikanov[1], A.M. Vorotynov[1], I.Yu. Filatova[2], V.S. Sulyaeva[2]

[1] Kirensky Institute of Physics, Federal Research Center KSV SB, Russian Academy of Sciences, Krasnoyarsk, Russia
[2] Nikolayev Institute of Inorganic Chemistry, Siberian Branch of the Russian Academy of Sciences, Novosibirsk, Russia
[3] Siberian State University of Railway Transport, Novosibirsk, Russia

E-mail: agm@iph.krasn.ru

Received September 3, 2025
Revised September 3, 2025
Accepted December 15, 2025

The $(MnS)_{1-x}(TiN)_x$ solid solutions have first been synthesized by cation-anion substitution on the basis of the isostructural heterovalent α-$Mn^{2+}S^2$ (antiferromagnetic semiconductor) and $Ti^{3+}N^{3-}$ (low-temperature superconductor) compounds with a NaCl-type cubic structure. It has been established that anions (S and N) in the $(MnS)_{1-x}(TiN)_x$ ($x < 0.10$) solid solutions generally retain their valence, while the substitution cation (Ti) can be in different valence states. Cation-anion substitution changes the valence band of the α-MnS matrix via the occurrence of the contribution of titanium d electrons in the vicinity of the Fermi level and reduces the magnetic susceptibility in the paramagnetic state without a significant change in the α-MnS Néel temperature; accordingly, the spin-flop transition in the low-temperature region becomes less pronounced.

Keywords: magnetically ordered materials, crystal growth, cation-anion substitution.

DOI: 10.61011/PSS.2026.01.63243.244-25

Active research field of strongly electron correlated system with a Mott transition are due to the various electronic phases and physical properties in correlated electron materials (from the insulator — metal transition up to superconductivity) [1]. The practical significance of this effects and the importance of studying its mechanism are stimulating the search for new compounds and its investigations. α-MnS and TiN are presented this class of the materials.

Alpha manganese monosulfide (α-MnS) is well-known among monosulfides of $3d$ elements [2,3] as the only substance that, similar to the MeO ($Me = $ Mn, Fe, Co, Ni) oxides, has a NaCl face-centered cubic (fcc) lattice (sp. gr. $Fm3m$), while the remaining $3d$-series monosulfides crystallize in a NiAs-type hexagonal structure. The TiN compound is formed in the same structural type (fcc, sp. gr. $Fm3m$) as α-MnS, but their physical properties are extremely different. At 300 K, the α-MnS is a paramagnetic Mott semiconductor with a high electrical resistivity ($\sim 10^5\,\Omega \cdot$ cm) and around 150 K it undergoes a magnetic transition to the antiferromagnetic state [4,5]. At applied magnetic fields in this sulfide the spin-flop transition with the anomalies of the dielectric and magnetostiction properties was found in the antiferromagnetic phase [5]. Bulk TiN samples exhibit a room-temperature electrical resistivity of $20 \div 40\,\Omega \cdot$ cm and, in the films of this compound, an insulator-superconductor transition in the low-temperature region was detected [6–9]. Additional differences between α-MnS and TiN lie in the fact that α-MnS is classified as an ionic compound with a 7% covalence admixture [10], whereas in TiN chemical bonds are covalent metallic [11]. Both MnS and TiN are considered to be promising for application [11–13].

Since MnS and TiN crystal structures are identical, one can expect the formation of a continuous series of α-MnS-TiN solid solutions with the composition-dependent physical properties. In contrast to the well-studied cation-substituted [14–17] and anion-substituted [18] manganese mono-sulfides, the investigation of α-MnS-TiN system elucidated the regularities of formation of cation-anion-substituted samples based on the matrix with a NaCl-type fcc lattice and the effect of changes in the nature of chemical bonds on the physical and functional properties.

This work presents the results of the synthesis and detailed investigations of the morphology, crystal structure, atomic charge state, and magnetic and resonance properties of the newly synthesized $(MnS)_{1-x}(TiN)_x$ ($x \leq 0.10$) single-crystal compounds.

1. Experimental methods

The $(MnS)_{1-x}(TiN)_x$ ($x = 0.01$, 0.03, 0.05, 0.10) single crystals were synthesized using the previously reported method for growing of the cation-substituted α-MnS single

crystals (for more detail, see [15–17]). At the first synthesis stage, powder samples were obtained. Single crystals up to 1 cm^3 in size were grown by spontaneous melt crystallization of the powder samples using induction heating in an argon flow. In order to determine the optimal procedure condition, three different experiments were performed for each composition.

The phase composition and the crystal structure of the obtained powder and single-crystal samples were controlled by X-ray diffraction (XRD) analysis. The C, H, N, and S contents in the $(MnS)_{1-x}(TiN)_x$ powder samples were measured by a standard method on a vario MICRO cube CHNS elemental analyzer. The morphology, elemental composition, and microstructure of the samples at high ($2000\times$) magnification were studied on a Jeol JSM 6700F scanning electron microscope at an accelerating voltage of 15 kV. The element mapping was performed using a Bruker Quantax 200 EDX spectrometer with a Bruker X-Flash 6|60 detector. The detector energy resolution was < 129 eV. The measured data were analyzed using the Esprit 2.1 software with the P/B-ZAF correction accounting for the background, atomic number, absorption, and secondary fluorescence.

X-ray photoelectron spectra (XPS) were obtained on a SPECS FleXPS spectrometer. X-ray excitation was used as an AlKα radiation source ($h\nu = 1486.6$ eV). The surface charge was taken into account from the position of the C1s line with a binding energy of 284.5 eV. The experimental XPS spectra were analyzed in the CasaXPS 2.3.15 software package. The accuracy of the binding energy measurement in the XPS spectra was 0.2 eV.

The electron paramagnetic resonance (EPR) spectra were measured in the temperature range of 77–300 K on an SE/X-2544 X-band EPR spectrometer at a frequency of 9.4 GHz. The magnetic properties of the samples were explored using a highly sensitive SQUID magnetometer in a magnetic field of 50 Oe, on a vibrating sample magnetometer (VSM) [19,20] at temperatures of 77–300 K, and on a Quantum Design PPMS-9 Physical Property Measurement System in the temperature range of 4.2–300 K and magnetic fields of up to 90 kOe.

2. Results and discussion

It is known [21,22] that the stability of the NaCl-type fcc lattice, in which the cation and anion have an octahedral environment, is determined by the valence, coordination number, and geometric sizes of ions involved in the formation of a substance. The stability condition for the second nearest neighbors of the NaCl lattice of the 6 coordination type is determined by the ratio r_{cat}/r_{an} between the cation and anion ionic radii and has the form $0.732 > (r_{cat}/r_{an}) > 0.414$, where r_{cat} and r_{an} are the cation and anion ionic radii. For the $Mn^{2+}-S^{2-}$ chemical bond in α-MnS, this ratio is $r_{cat}/r_{an} = c = 0.5$, which corresponds to the stability condition of the NaCl-type lattice with sulfur and manganese ions located in the octahedral sites. In the case of the $(MnS)_{1-x}TiN_x$ solid solution, it is necessary to take into account the possible formation of pairs of chemical bonds: $Ti^{2+}-S^{2-}$ (r_{cat}/r_{an}) $= c = 0.428$), $Ti^{2+}-N^{3-}$ ($c = 0.527$), $Ti^{3+}-N^{3-}$ ($c = 0.466$), and $Mn^{3+}-N^{3-}$ ($c = 0.47$). In the estimation, the data on the ionic radius from [21, p. 139] were used. All the considered valence pairs meet the NaCl structure stability condition and can exist in the $(MnS)_{1-x}(TiN)_x$ solid solutions. However, in the case of 12 nearest neighbors, the binary structure factor is unknown. In addition, although the ratio between the ionic radii for the $Ti^{2+}-S^{2-}$ ionic pair ($r_{cat}/r_{an} = 0.428$) corresponds to the NaCl fcc structure stability ratio, the TiS sulfide has a hexagonal NiAs structure [23,24].

Table 1. Data of the CHNS analysis of the $(MnS)_{1-x}(TiN)_x$ powder sample (wt.%)

x	N	S	H
0.01	0.2	35.4	< 0.2
0.03	0.9	37.6	< 0.2
0.05	1.6	33.4	< 0.2
0.1	1.4	36.4	< 0.2

For the stoichiometric α-MnS composition (63.1 wt.% of Mn and 36.9 wt.% of S) with a lattice parameter of $a = 5.224$ Å [4], the characteristic interionic spacings are Mn–S = 2.61 Å and Mn–Mn = 3.69 Å. Similar to the α-MnS_x [24] and TiO_x [25] minerals, titanium nitride TiN_x represents an interstitial phase with the homogeneity region from 14.8 to 22.6 wt.% of nitrogen, which corresponds to the $TiN_{0.6}$ and $TiN_{1.0}$ formulas ($Ti_{1.4}N$–TiN) [26,27]. For the stoichiometric titanium nitride composition (77.4 wt.% of Ti and 22.6 wt.% of N), the lattice parameter is $a = 4.2346$ Å and the interionic spacings in the bulk phase are Ti–N = 2.12 Å and Ti–Ti = 3.0 Å.

The most accurate method for determining the chemical composition of anions in a substance is the CHNS analysis, which allows simultaneous determination of the contents of light chemical elements (carbon, hydrogen, nitrogen, and sulfur). Table 1 gives the analysis results of the C, H, N, and S contents determined by this method, which indicate the presence of sulfur and nitrogen ions in $(MnS)_{1-x}(TiN)_x$ ($x \leq 0.10$) powder samples. The elemental composition of the $(MnS)_{1-x}(TiN)_x$ samples with different cation substitution degrees x is given in Table 2 and Table 3.

Figure 1 shows a typical SEM images of the $(MnS)_{1-x}(TiN)_x$ synthesized crystals and its chemical element distribution maps. According to the EDX analysis data, all investigated samples contain Ti, Mn, S, and N. At low concentrations ($x \leq 0.03$), the element distribution maps demonstrate a uniform elemental distribution. However, as the degree of cation substitution increases to $x = 0.05^*$ (Figure 1, *d*), heterogeneity areas related to the formation of the additional TiN phase.

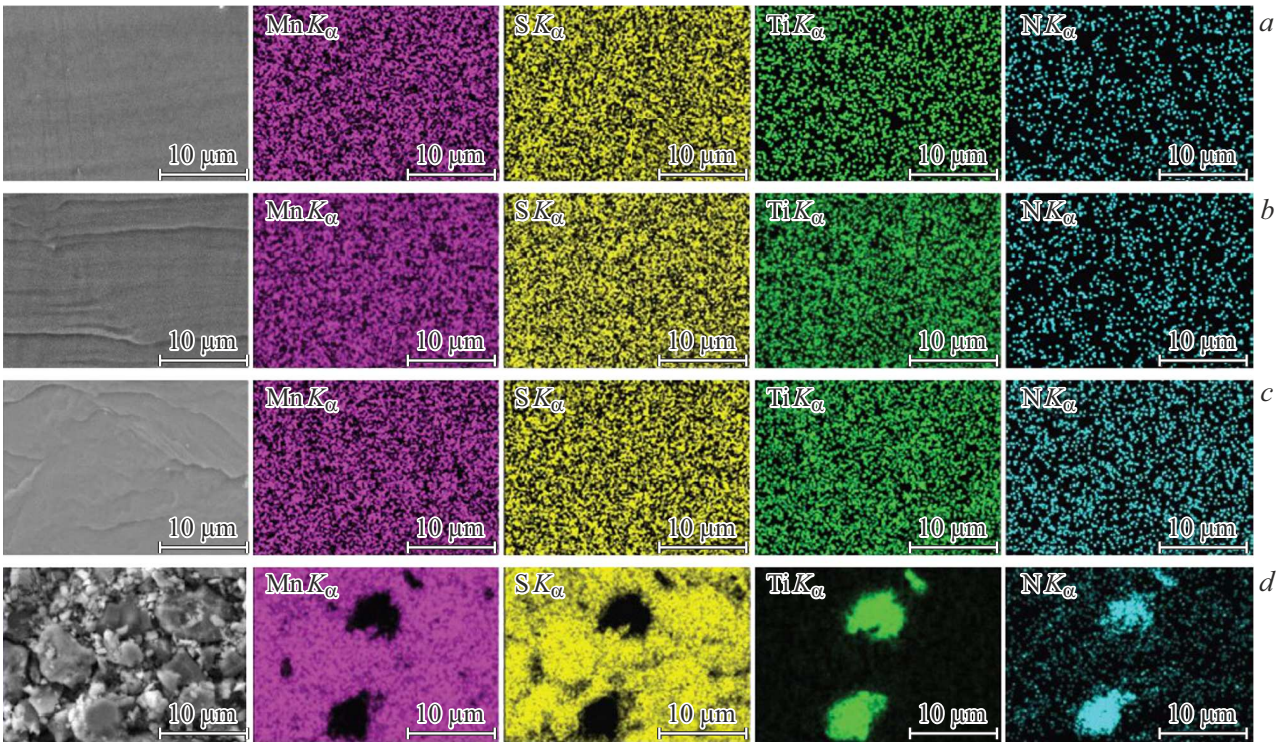

Figure 1. SEM images of $(MnS)_{1-x}(TiN)_x$ samples with $x =$ (*a*) 0.01, (*b*) 0.03, (*c*) 0.05, and (*d*) 0.05*.

In order to determine the valence state of ions included in $(MnS)_{1-x}(TiN)_x$ substances, the XPS spectra were analyzed. The Mn3*s* and sulfur S2*p* spectra measured on the samples with $x = 0.01$ and 0.05 showed that under the cation-anion substitution, the electron density distribution and charge state of manganese and sulfur ions remain divalent, which is typical of manganese monosulfide and cation-substi-tuted compounds based on it [14].

Table 2. Elemental composition of the $(MnS)_{1-x}(TiN)_x$ ($x < 0.1$) powder sample

Element	Degree of substitution x, wt.%		
	0.01	0.03	0.05
Mn	64.61 ± 1.75	64.89 ± 1.7	62.33 ± 1.7
S	34.38 ± 1.14	34.36 ± 1.12	34.4 ± 1.17
Ti	1.00 ± 0.06	0.73 ± 0.05	3.27 ± 0.05
N	0 ± 0.01	0.03 ± 0.01	1 ± 0.01

Table 3. Elemental composition of the $(MnS)_{1-x}(TiN)_x$ (x= 0.05*) composite sample

Element	Content, wt.%
Mn	59.28 ± 1.7
S	32.22 ± 1.12
Ti	2.2 ± 0.05
N	0.6 ± 0.01

Figures 2 and 3 show the nitrogen N1s and the titanium Ti2*p* spectral lines for $(MnS)_{1-x}(TiN)_x$ samples with $x = 0.01$ and 0.05. The valence state of ions in titanium nitride is $Ti^{3+}N^{3-}$. For this substance, the binding energy of the N1*s* line is ~ 397 eV. For the $(MnS)_{1-x}(TiN)_x$ compound, the N1*s* line (Figure 2, the curve *3*) lies in the wide binding energy range of 397–400 eV, as observed for MnS nanoparticles with the nitrogen impurity [28] or titanium-doped aluminum nitride $Al_{1-x}Ti_xN$ [29]. Thus one can conclude that nitrogen ions in the MnS matrix retain the trivalent state. The measured Ti2*p* spectra (Figure 3) of $(MnS)_{1-x}(TiN)_x$ samples represent a superposition of two sets ($2p_{3/2}$, $2p_{1/2}$ spin doublets) related to titanium ions of different types (the red (I) and blue (II) curves on Figure 3). The binding energy of low-energy component I corresponds to the divalent state of titanium ions with the binding energy of TiS and TiO. The binding energy of component II corresponds to the trivalent state of titanium ions (TiN, $Ti2p_{3/2} \sim 462$ eV) [30]). An increase in the degree of cation-anion substitution (x) in $(MnS)_{1-x}(TiN)_x$ leads to a decrease in the intensity of component I relative to component II, which indicates a change in the nature of the chemical bonding of titanium atoms and an increase in the concentration of trivalent titanium ions. The analysis of N1s nitrogen and Ti2*p* titanium lines allows one to conclude that the cation-anion substitution in the $(MnS)_{1-x}(TiN)_x$

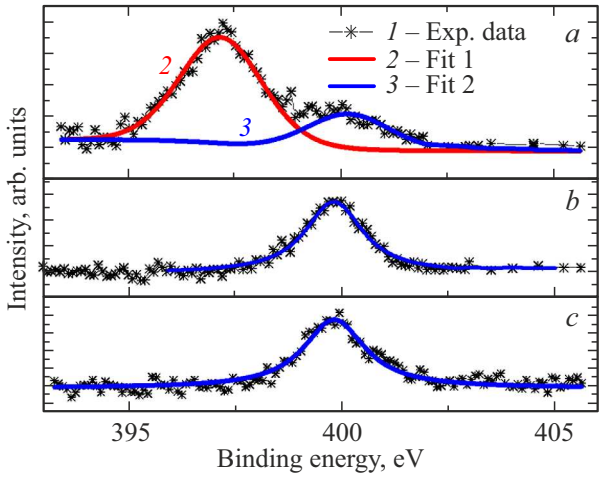

Figure 2. The N1s nitrogen spectra for $(MnS)_{1-x}(TiN)_x$ samples: (a) powder, $x = 0.01$; (b) single crystal, $x = 0.01$; and (c) single crystal, $x = 0.05$. Points show the experimental data and curves, the result of data analysis.

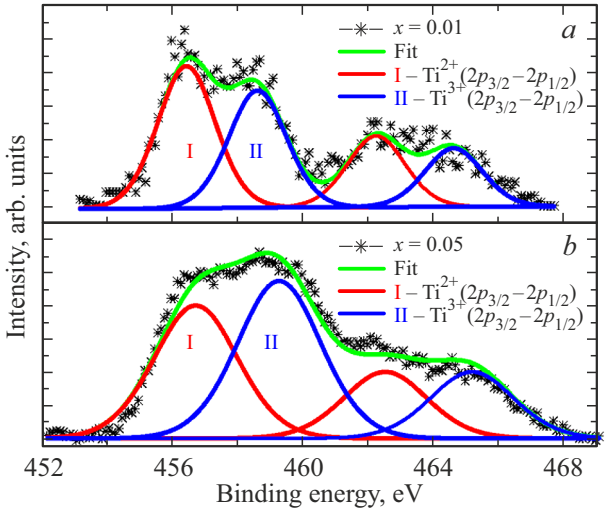

Figure 3. The Ti2p titanium spectra for $(MnS)_{1-x}(TiN)_x$: (a) powder, $x = 0.01$ and (b) single crystal, $x = 0.05$. Points show the experimental data and curves, the results of data analysis.

compounds at a low substitution degree ($x = 0.01$) leads to the formation of chemical bonding of two types: Ti–S and Ti–N. The contribution of Ti–N bonds increases with the degree of substitution.

Figure 4 shows the typical X-ray powder diffraction patterns of synthesized $(MnS)_{1-x}(TiN)_x$ samples measured at room temperature (300 K). Figure 4, a corresponds to the sample with $x = 0.03$ with a uniform nitrogen and titanium distribution over the single crystal volume. Figures 4, b and 4, c present X-ray powder diffraction patterns for the $(MnS)_{1-x}(TiN)_x$ samples with $x = 0.05$ and 0.05^*. A halo (blurred peak) in the grazing angle region around 41.62° (Figure 4, b) indicates the presence of TiN_x nanoinclusions in the obtained samples. The X-ray diffraction pattern of the samples with $x = 0.05^*$ (Figure 1, c) contains the additional (111) and (200) reflections, which indicate the formation of single-crystal TiN_x spacers in $(MnS)_{1-x}(TiN)_x$ crystals. The size of TiN_x nano- and micro planes and their amount in $(MnS)_{1-x}(TiN)_x$ single crystals depend on the crystallization temperature and time, and can be tuned.

It was established by XRD analysis that the obtained $(MnS)_{1-x}(TiN)_x$ solid solutions have a NaCl-type crystal structure similar to the structure of the initial α-MnS matrix (sp. gr. $Fm3m$, Mn in the 4a (0, 0, 0) site and S in the 4b (0.5, 0.5, 0.5) site, JCPDS-ICDD card data, N06-0518, $a = 5.224$ Å). The lattice parameters of the $(MnS)_{1-x}(TiN)_x$ compounds upon variation in the composition (x value) changes from $a = 5.217 \pm 0.01$ Å at $x = 0.01$ to $a = 5.211 \pm 0.01$ Å at $x = 0.05$. A decrease in the lattice parameter of the sample indicates the cation-anion substitution, since the divalent titanium ion (Ti^{2+}, d^2s^4, $S = 1$) in the octahedral position has an ionic radius of 1 Å, while for Ti^{3+} (Ti^{3+}, d^1s^4, $S = 1/2$), the ionic radius in the octahedral position of the cubic lattice is 0.87 Å [26,27].

It is known that the α-MnS molar magnetic susceptibility at 300 K is 0.00539 cm^3/mol (0.000062 cm^3/g) [5]; for TiN, this quantity amounts to $38 \cdot 10^{-6}$ cm^3/mol ($0.6 \cdot 10^{-6}$ cm^3/g) [9]. The paramagnetic properties of $(MnS)_{1-x}(TiN)_x$ single crystals in the temperature range of 160–300 K were confirmed by the electron paramagnetic resonance (EPR) study. In Figure 5, the EPR data on the single-crystal $(MnS)_{1-x}(TiN)_x$ samples are compared with the data for α-MnS. It was established that, at a low degree of cation-anion substitution, the resonance properties of the homogeneous $(MnS)_{1-x}(TiN)_x$ single crystals are similar to the data typical of the paramagnetic state of manganese monosulfide with the NaCl (fcc) structure. The EPR signal has a Lorentzian shape with the g factor changing within

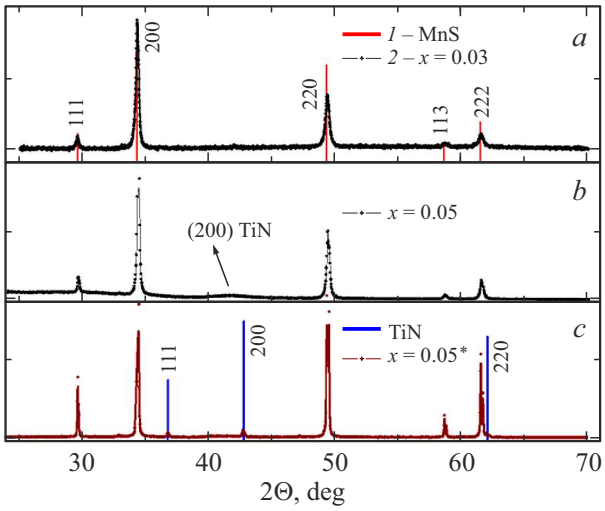

Figure 4. The X-ray diffraction patterns of $(MnS)_{1-x}(TiN)_x$ powder samples with: (a) $x = 0.03(2)$ and (b) $x = 0.05$ containing TiN nanoparticles and (c) $x = 0.05^*$ with single-crystal TiN spacers. Vertical solid lines in Figures 4, a and 4, c show reference data for MnS and TiN, respectively.

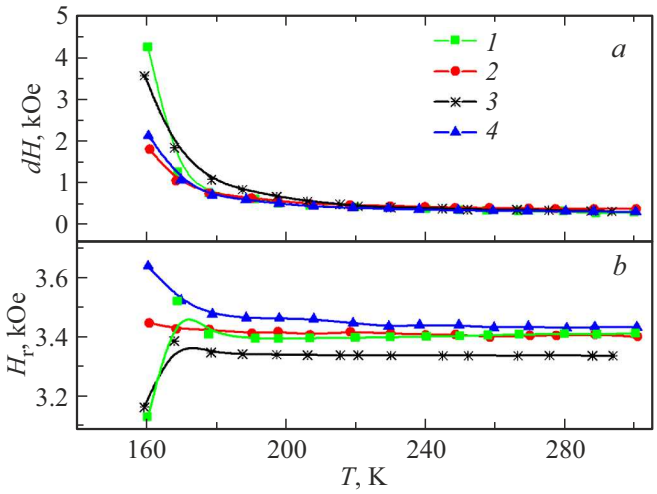

Figure 5. Temperature dependences of (*a*) the EPR line width and (*b*) resonance field for the $(MnS)_{1-x}(TiN)_x$ single crystals: (*1*) MnS, (*2*) $x = 0.01$, (*3*) $x = 0.03$, and (*4*) $x = 0.05$

.

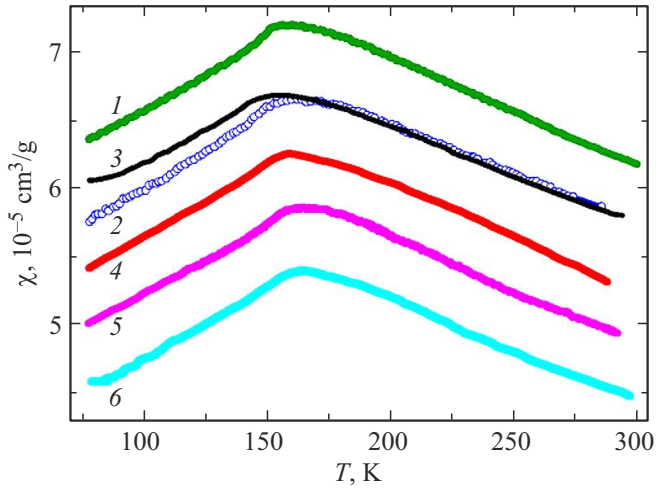

Figure 6. The temperature dependences of magnetic susceptibility for $(MnS)_{1-x}(TiN)_x$ single- crystal samples in the range of 77–300 K. (*1*) MnS, (*2*) $x = 0.01$ ($H = 50$ Oe), (*3*) $x = 0.01$ ($H = 1$ kOe), (*4*) $x = 0.03$ ($H = 100$ Oe), (*5*) $x = 0.05$, and (*6*) $x = 0.05^*$.

1.98–2.05 characteristic of the divalent manganese ion in the octahedral position of the NaCl lattice. In the region of 160–170 K, the EPR line broadening (Figure 5, *a*) and Hr resonance field anomaly (Figure 5, *b*) are observed, indicating the antiferromagnetic transition in the α-MnS matrix.

Figure 6 presents temperature dependences of the magnetic susceptibility χ of the $(MnS)_{1-x}(TiN)_x$ crystals around $77 \div 300$ K. The paramagnetic molar susceptibility of the crystals at 300 K ranges within $0.00501 \div 0.0046$ cm^3/mol and is lower than that of the initial α-MnS matrix (0.00546 cm^3/mol). According to the EPR spectroscopy data, $(MnS)_{1-x}(TiN)_x$ crystals are antiferromagnets with a Néel temperature T_N (maximum in the $\chi(T)$ dependence) weakly dependent on the crystal composition (the x value): 150–160 K. In the paramagnetic state $T \le T_N$, the $\chi(T)$ dependences for the $(MnS)_{1-x}(TiN)_x$ samples are described by the Curie–Weiss law. The effective magnetic moment $\mu(\mu_B)$ and the paramagnetic Néel temperature Θ(K) of the $(MnS)_{1-x}(TiN)_x$ compound change from $6\mu_B$ and -650 K (at $x = 0.01$) to $4.9\mu_B$ and -540 K at $x = 0.05$. In general, the change in the magnetic properties of the $(MnS)_{1-x}(TiN)_x$ samples under the cation-anion substitution is similar to their change in the $Cu_xMn_{1-x}S$ [15] and $Al_{1-x}Ti_xN$ systems [29].

Figure 7 shows the field dependence of the magnetization for $(MnS)_{1-x}(TiN)_x$ ($x = 0.03$) crystal in a magnetic field of up to 90 kOe at $T = 4.2$ K. The measured data show that, in the low-temperature region, the sample exhibits a change in the magnetization in a magnetic field that is similar to spin-flop transitions. The insets in Figure 7 show the field dependence of the differential magnetic susceptibility dM/dH (the upper left corner of the plot) and the field dependence of the magnetization at $T = 300$ K (the lower right corner of the plot).

In contrast to α-MnS [4], in the cation-anion-substituted $(MnS)_{1-x}(TiN)_x$ crystals, the spin-flop transition is continuous, which can be due to a change in their domain structure caused, for example, by a change in the elastic parameters of the crystals.

Figure 8 shows the valence band spectra of the investigated $(MnS)_{1-x}(TiN)_x$ solid solutions. A broad maximum in the energy range of $0 \le 9$ eV is determined by the contributions of the overlapping bands of the titanium and manganese $3d$ states with the sulfur $3p$ states, with the most intense maximum in the binding energy region around ~ 4 eV related to the contributions of the manganese $3d$ states; the energies of the titanium $3d$ states are closer to

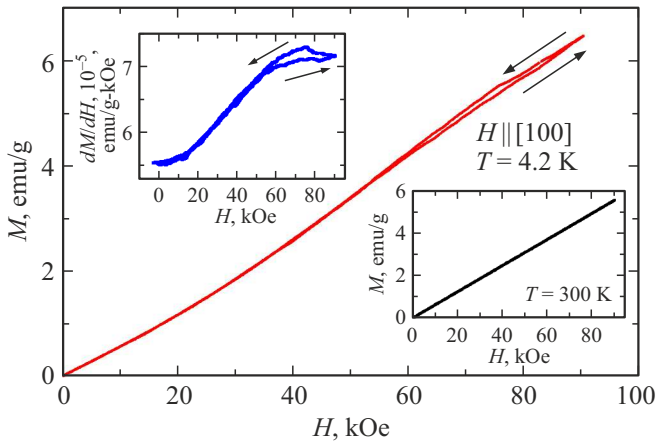

Figure 7. Field dependence of the magnetization of $(MnS)_{1-x}(TiN)_x$ crystal with $x = 0.03$ in a magnetic field of up to $H = 90$ kOe and $T = 4.2$ K. Inserts: field dependences of differential susceptibility dM/dH at 4.2 K (left upper corner) and magnetization at 300 K (right lower corner).

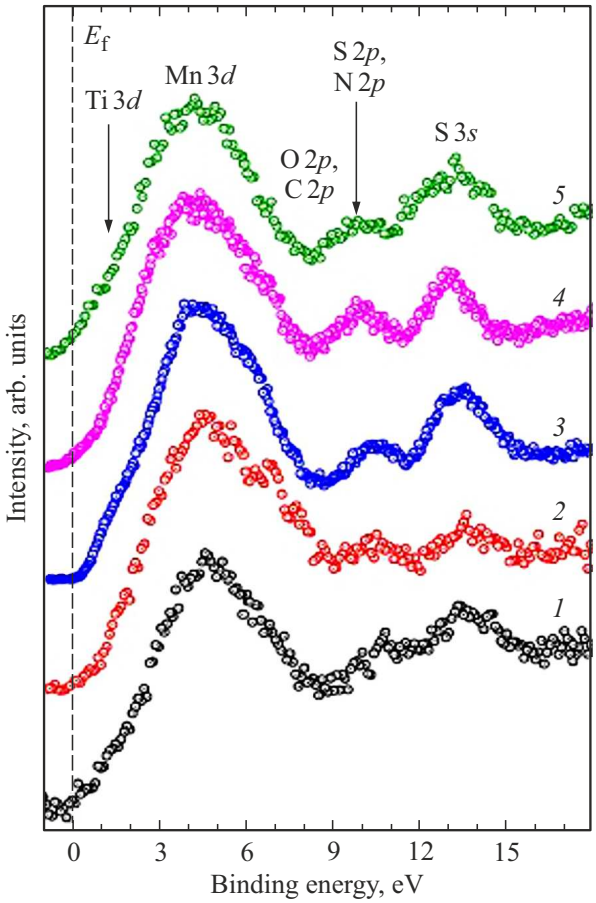

Figure 8. Valence band for the initial matrix and $(MnS)_{1-x}(TiN)_x$: (*1*) MnS-matrix, (*2*) $x = 0.01$ (powder), (*3*) $x = 0.01$ (single crystal), (*4*) $x = 0.05$ (powder), (*5*) $x = 0.05$ (single crystal).

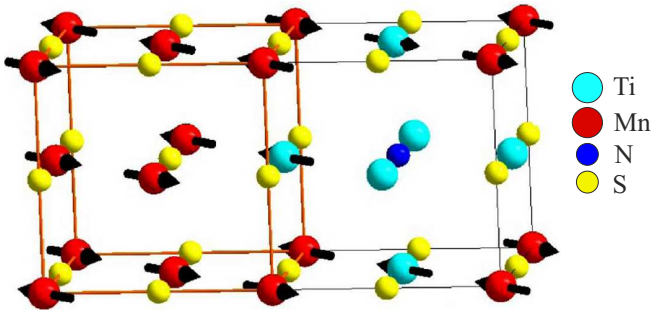

Figure 9. Formation of the cation clusters NTi_6 and SMn_6 in the $(MnS)_{1-x}(TiN)_x$ single crystals.

the Fermi level. The maximum in the binding energy region around 9–12 eV is related to the contributions of the sulfur and nitrogen $2p$ states. In the depth of the valence band, at a binding energy of ~ 13 eV, the sulfur $3s$ states and the manganese $3p$ states are localized.

It follows from the comparison of the experimental results of $(MnS)_{1-x}(TiN)_x$ compounds (Figure 8) with the literature data on MnS and TiN that the cation-anion substitution causes a significant change in the nature of the valence band of the manganese monosulfide matrix due to the formation of the titanium d band in the vicinity of the Fermi level. In addition, one can expect a change in the electrical properties of $(MnS)_{1-x}(TiN)_x$ compounds. The test measurements showed that the electrical resistance of the samples with $x = 0.05^*$ is three orders of magnitude lower than that for α-MnS.

The obtained experimental data show that even a low degree of the cation-anion substitution in the homogeneous MnS matrix with a NaCl-type cubic structure induces a change in the charge state and the electronic and magnetic properties of $(MnS)_{1-x}(TiN)_x$ compounds. The spatial topology of $(MnS)_{1-x}(TiN)_x$ crystals is determined not only by the size and valence of ions, but also by the nature (ionic covalent) of the chemical bonds, as well as by the distribution of these bonds over the crystal. The short-range order (coordination 12) most likely plays a more important role in changing the physical properties of the samples than the coordination of the second nearest neighbors (coordination 6). This points out the importance of the local structural order in the $(MnS)_{1-x}(TiN)_x$ single crystals (random atomic displacements and nonuniform crystal lattice distortion) and the possibility of controlling this order by external factors.

The established features in the formation of the microstructure and valence state of ions in the $(MnS)_{1-x}(TiN)_x$ single crystals suggest that the most probable model explaining the behavior of their physical properties is the magic cluster model [30,31]. The $(MnS)_{1-x}(TiN)_x$ compound formed as a result of the cation-anionic substitution can be presented as randomly distributed and disordered $(Mn^{2+})S_6$, $(Ti^{3+})N_6$, and $(Ti^{2+})S_6$ heterovalent octahedra, the detailed packing of which in a crystal depends on both the substitution degree and the chosen temperature and time mode of the crystal growth. Cluster formalism [30,31] takes into account the local point symmetry of cations and assumes the replacement of the cation-anion system by a lattice with the MnS_6 or SMn_6 clusters localized in its nodes, the electronic structure of which efficiently takes into account the p–d covalence. One of the possible types of cluster formation in the single-crystal $(MnS)_{1-x}(TiN)_x$ compounds is illustrated in Figure 9.

3. Conclusion

Thus, powder and single crystals of the new $(MnS)_{1-x}(TiN)_x$ compounds were first synthesized. The modes of the synthesis of homogeneous and heterogeneous crystals with a NaCl-type cubic structure were determined. It was established that the cation-anion substitution in the system of α-MnS-TiN isostructural compounds with different valence states of cations and anions (α-$Mn^{2+}S^{2-}$ and $Ti^{3+}N^{3-}$) is accompanied by the formation of the mixed disordered $(MnS)_{1-x}(TiN)_x$ solid solutions, in which anions

generally retain their valence, while the substitution cation can be in different valence states.

In the temperature range of $77 \div 300$ K, the crystal structure and the resonance and magnetic properties of $(MnS)_{1-x}(TiN)_x$ crystals are generally similar to the properties of the α-MnS matrix. An increase in the degree of cation-anion substitution and a change in the nature of chemical bonds in $(MnS)_{1-x}(TiN)_x$ compounds are accompanied by a significant change in its electronic structure and a decrease in the magnetic susceptibility in the paramagnetic state of the matrix at 300 K without a serious change in its Néel temperature. The cation-anion substitution changes the nature of the spin-flop transition observed in α-MnS in the low-temperature region (4.2 K).

The results of the experimental investigations of the chemical composition and the electronic, resonance, and magnetic properties allowed us to conclude that study of the physical properties of $(MnS)_{1-x}(TiN)_x$ compounds in a wide range of temperatures and magnetic and electric fields is promising for determining the possibility of the development of randomly distributed environments for micro- and nanoelectronics on their basis.

Acknowledgments

We thank the researches of the Shared Facilities Center of the Krasnoyarsk Scientific Center (Krasnoyarsk, Russia) for help in our experiments.

Funding

This study was supported by ongoing institutional funding (The basic project of the Kirensky Institute of Physics, Federal Research Center „Krasnoyarsk Scientific Center" Siberian Branch of the Russian Academy of Sciences). No additional grants to carry out or direct this particular research were obtained.

Conflict of interest

There are no conflicts to declare

References

[1] P.A. Lee, N. Nagaosa, X.-G. Wen. Rev. Mod. Phys. **78**, *1*, 17 (2006). htpps://doi.org/10.1103/RevModPhys.78.17
[2] G.V. Samsonov, S.V. Drozdova. Sul'fidy. Metallurgiya, M. (1972) (in Russian).
[3] G.V. Loseva, S.G. Ovchinnikov, G.A. Petrakovsky. Perekhod metall–dielektrik v sul'fidah 3d-metallov. Nauka, Novosibirsk (1983). p. 144 (in Russian).
[4] J.J. Banewicz, R. Lindsay. Phys. Rev. **104**, *2*, 318 (1956). htpps://doi.org/10.1103/PhysRev.104.318
[5] G.M. Abramova, A.L. Freidman, S.A. Skorobogatov, A.M. Vorotynov, S.M. Zharkov, S. Molokeev, A.I. Pankrats. JETP **138**, *3*, 398 (2024).
[6] A. Valour, M.A. Usuga Higuita, G. Guillonneau, N. Crespo-Monteiro, D. Jamon, M. Hochedel, J.-Y. Michalon, S. Reynaud, F. Vocanson, C. Jiménez, M. Langlet, C. Donnet, Y. Jourlin. Surf. Coat. Technol. **413**, 127089 (2021). https://doi.org/10.1016/j.surfcoat.2021.127089
[7] R. Patsalas, N. Kalfagiannis, S. Kassavetis, G. Abadias, D.V. Bellas, Ch. Lekka, E. Lidorikis. Mater. Sci. Eng.: R.: Rep. **123**, 1 (2018). https://doi.org/10.1016/j.mser.2017.11.001
[8] N. Hadacek, M. Sanquer, J.-C. Villégier. Phys. Rev. B **69**, *2*, 024505 (2004). https://doi.org/10.1103/PhysPevB.69.024505
[9] W. Tsai, M. Delfino, J.A. Fair, D. Hodul. J. Appl. Phys. **73**, *9*, 4462 (1993). https://doi.org/10.1063/1.352785
[10] B.E.F. Fender, A.J. Jacobson, F.A. Wedgwood. J. Chem. Phys. **48**, *3*, 990 (1968). https://doi.org/10.1063/1.1668855
[11] U. Mahajan, M. Dhonde, K. Sahu, P. Ghosh, P.M. Shirage. Mater. Adv. **5**, *3*, 846 (2024). https://doi.org/10.1039/D3MA00965c
[12] R.B. Pujari, A.C. Lokhande, A.A. Yadav, J.H. Kim, C.D. Lokhande. Mater. Design **108**, 510 (2016). https://doi.org/10.1016/j.matdes.2016.07.038
[13] C.C. Chang, J. Nogan, Z.-P. Yang, W.J.M. Kort-Kamp, W. Ross, T.S. Luk, D.A.R. Dalvit, A.K. Azad, H.-T. Chen. Sci. Rep. **9**, *1*, 15287 (2019). https://doi.org/10.1038/s41598-019-51236-3
[14] M.M. Syrokvashin, E.V. Korotaev, N.A. Kryuchkova, V.V. Zvereva, I.Yu. Filatova, A.V. Kalinkin. Appl. Surf. Sci. **492**, 209 (2019). https://doi.org/10.1016/j.apsusc.2019.05.237
[15] G.M. Abramova, G.A. Petrakovskii, V.V. Sokolov, D.A. Velikanov, A.M. Vorotynov, A.F. Bovina, A.A. Amirov, A.M. Aliev, L.N. Khanov, G.S. Patrin. Phys. Solid State **54**, *3*, 531 (2012). https://doi.org/10.1134/S106378341203002X
[16] G.M. Abramova, A. Hanzawa, T. Kagayama, Y. Mita, E.V. Eremin, G.M. Zeer, S.M. Zharkov, S.G. Ovchinnikov. J. Magn. Magn. Mater. **465**, 775 (2018). https://doi.org/10.1016/j.jmmm.2018.05.056
[17] G. Abramova, J. Schefer, N. Aliouane, M. Boehm, G. Petrakovskiy, A. Vorotynov, M. Gorev, A. Bovina, V. Sokolov. J. Alloy. Compd. **632**, 563 (2015). http://dx.doi.org/10.1016/j.jallcom.2015.01.162
[18] C.-H. Huang, C.-W. Wang, C.-C. Chang, Y.-C. Lee, G.-T. Huang, M.-J. Wang, M.-K. Wu. J. Mag. Magn. Mater. **483**, 205 (2019). https://doi.org/10.1016/j.jmmm.2019.03.105/
[19] D.A. Velikanov. Inorg. Mater. Appl. Res. **11**, *4*, 801 (2020). https://doi.org/10.1134/S2075113320040413
[20] D.A. Velikanov. RF Patent, RU2481591 (C1). Byull. No. 13, 10.05.2013. https://worldwide.espacenet.com/patent/search?q=RU2481591
[21] M.P. Shaskolskay. Kristallographie (Moscow, 1976, 392 p.)
[22] G.V. Bokiy. Crystal Chemistry (Nauka, Moscow, 1971, 400 p.)
[23] F. Jellinek. Arkiv. Kemi **20**, 447 (1963).
[24] L.L. Lewis, L.L. Goodenough. J. Solid State Chem. **114**, *2*, 342 (1995). https://doi.org/10.1006/jssc.1995.1054
[25] A.A. Valeeva, A.I. Gusev. Phys. Solid State **66**, *5*, 761 (2024). DOI:10.61011/PSS.2024.05.58510.66
[26] G.V. Samsonov. Nitridy. Naukova dumka, Kiev (1969). p. 380 (in Russiasn).

[27] R.D. Shannon. Acta Crystallographica A **32**, 751 (1976). https://doi.org/10.1107/S0567739476001551
[28] S. Li, J. Chen, J. Xiong, X. Gong, J. Ciou, P.S. Lee. Nano-Micro Lett. **12**, *1*, 34 (2020). https://doi.org/10.1007/s40820-020-0367-9
[29] M. Magnuson, M. Mattesini, S. Li, C. Höglund, M. Beckers, L. Hultman, O. Eriksson. Phys. Rev. B **76**, *19*, 195127 (2007). https://doi.org/10.1103/PhysRevB.76.195127
[30] A.D. Lewoczko, J.J. BelBruno, S.T. Bromley. Chem. Phys. Lett. **556**, 207 (2013). http://doi.org/10.1016/j.cplett.2012.11.049
[31] A.S. Moskvin. Magnetochemistry **9**, 224 (2023); JETF **167**, 412 (2025). DOI: 10.31857/S0044451025030125.